AIAA JOURNAL
Vol. 42, No. 11, November 2004

Analysis of Magnetohydrodynamic Control of Scramjet Inlets

Mikhail N. Shneider,* Sergey O. Macheret,† and Richard B. Miles‡
Princeton University, Princeton, New Jersey 08544

Magnetohydrodynamic (MHD) control of forebody flow compression and air mass capture in scramjet inlets is analyzed for flight at Mach 5–10. Because of the low static temperature, nonequilibrium electrical conductivity is created by electron beams injected into the gas along magnetic field lines. Two-dimensional inviscid steady-state flow equations are solved jointly with equations describing electron-beam-induced ionization profiles, plasma kinetics, and MHD effects. Among several scenarios considered, the scenario with an MHD accelerator has only disadvantages. A modest increase in mass capture can in principle be accomplished with a Faraday MHD generator, if the magnetic field has components both parallel and orthogonal to the flow. The principal focus is on MHD inlet control at flight Mach numbers higher than the design value. The shocks that would otherwise enter the inlet can be moved back to the cowl lip by placing an MHD generator at one of the compression ramps. Analysis shows that the best performance of such a device is achieved with a very short MHD region placed as far upstream (close to the vehicle nose) as possible, in conjunction with a high-current ionizing electron beam. An MHD energy bypass scenario with on-ramp MHD generator for inlet control is briefly discussed.

I. Introduction

THE geometry, size, and weight of scramjet-powered hypersonic vehicles are largely dictated by the need to compress the ambient low-density air upstream of the combustor.[1] The optimum geometry corresponds to the well-known shock-on-lip (SOL) condition (Fig. 1): The compression ramp shocks converge on the cowl lip and the reflected shock impinges on the upper boundary of the inlet.[1] Because shock angles are determined by the flight Mach number, the SOL condition cannot be met at Mach numbers higher or lower than the design Mach number.[1] At Mach numbers higher than the design value, the shocks move inside the inlet (Fig. 2), causing multiple reflected shocks, loss of stagnation pressure, possible boundary-layer separation, and engine unstart. At Mach numbers lower than the design value, a portion of the air compressed by the shock misses the inlet (spillage) and the air mass capture decreases (Fig. 3).

To avoid performance penalties at off-design Mach numbers, a variable geometry inlet can be used. However, the mechanical variable geometry system would be quite heavy, weighing perhaps tens of metric tons. An alternative approach is to optimize inlets using energy addition to or extraction from the flow. Plasmas and various MHD devices may offer a viable optimization scheme.

One method of MHD control is to design the vehicle for a high Mach number, for example, Mach 10, and to decrease or eliminate the flow spillage at Mach numbers lower than the design value by an MHD accelerator device placed at one of the compression ramps (Fig. 4).[2] A significant disadvantage of this method compared with the MHD generator method shown in Fig. 5 is that the accelerator requires a substantial amount of power. In addition, due to joule heating by the MHD current and heat deposited by the conductivity-sustaining electron beam, there is a considerable stagnation pressure loss. Our recent analysis[2] demonstrated that the accelerator scenario not only involves substantial power consumption, but, in fact, reduces the mass capture due to gas expansion caused by the joule heating.

Another, recently suggested,[3] method of MHD inlet control is to operate an on-ramp MHD device in generator mode, using a magnetic field configuration with B field components both parallel and orthogonal to the flow (Fig. 6). According to Kuranov et al.,[3] air mass capture at Mach numbers lower than the design value can be increased with this method. Our recent calculations[2] showed that this method can, under certain specific conditions and assumptions, result in a modest increase in mass capture. If the electron beam-induced ionization profile is assumed either uniform or to have a Gaussian distribution along a slab region that extends vertically down from the ramp but does not reach the cowl level, then mass capture, total pressure coefficient, and compression ratio would actually all decrease.[2] The negative performance is due to joule heating and power introduced by the beam, resulting in entropy generation and thermal expansion. The positive effect of the compressing force $(\boldsymbol{j} \times \boldsymbol{B})_z = -j_y B_x$ is too weak to overcome the thermal expansion; no less important is that this force does not act on the gas below the ionized slab. If, however, a uniform electron beam power deposition is assumed through a slab region that extends vertically down to infinity, the mass capture and compression ratio increase slightly, although stagnation pressure decreases in about the same proportion as the mass capture increase.[2] Note that most of the ionized region in the slab is useless or even detrimental for the task of mass capture increase. It is only the combined effect of heating and the $(\boldsymbol{j} \times \boldsymbol{B})_z = -j_y B_x$ force on the gas region at the cowl level and below it that deflects streamlines and increases mass capture.

The fact that it is the heating at or below the cowl level that is most effective in scooping more air into the inlet allowed us to suggest a virtual cowl concept of increasing the mass capture.[2,4] The essence of the method is to create a heated region upstream of and somewhat below the cowl lip (Fig. 7). The incoming flow is deflected by the elevated-temperature and/or elevated-pressure region, causing an increased mass flow into the inlet. The heated region may be generated by supplying microwave or rf energy to a volume preionized by a focused laser or electron beam. Other possible means include plasma or hot-air jets and external combustion. An important advantage of the new method is that the air entering the inlet experiences little or no joule heating. Thus, stagnation pressure losses can be minimized. Moreover, with the right positioning of the virtual cowl, the stagnation pressure at the inlet throat can even be increased. The virtual cowl method can have an additional advantage of increased lift. A detailed quantitative analysis of the virtual cowl concept is presented elsewhere.[4]

Presented as Paper 2003-0170 at the AIAA 41st Aerospace Sciences Meeting, Reno, NV, 6–9 January 2003; received 20 July 2003; revision received 2 May 2004; accepted for publication 1 June 2004.

*Research Scientist, Department of Mechanical and Aerospace Engineering, D-414 Engineering Quadrangle. Senior Member AIAA.

†Senior Research Scientist, Department of Mechanical and Aerospace Engineering, D-414 Engineering Quadrangle; macheret@princeton.edu. Associate Fellow AIAA.

‡Professor, Department of Mechanical and Aerospace Engineering, D-414 Engineering Quadrangle. Fellow AIAA.

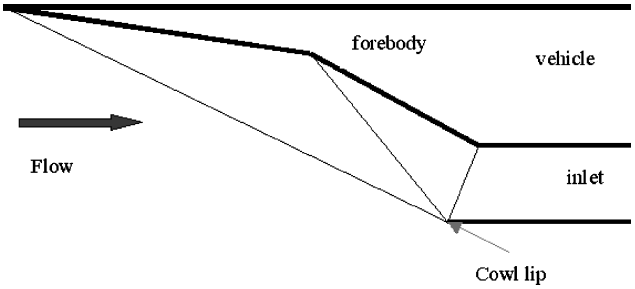

Fig. 1 Design forebody and inlet geometry with SOL condition.

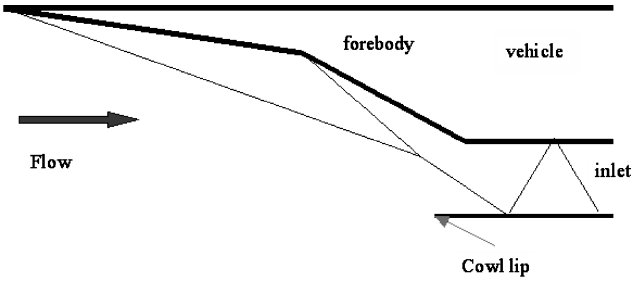

Fig. 2 Flow and shock geometry at Mach number higher than the design value, with no MHD control.

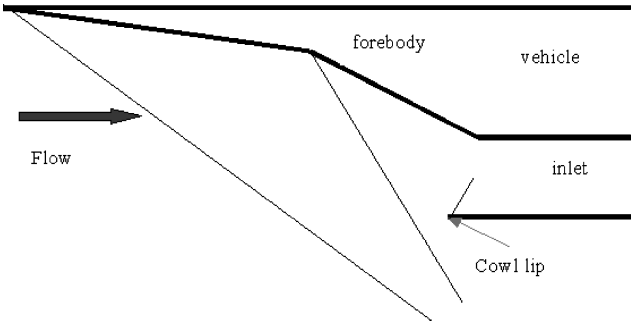

Fig. 3 Flow and shock geometry at Mach number lower than the design value, with no MHD control.

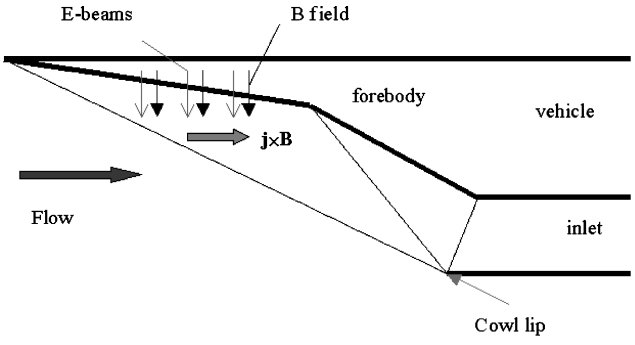

Fig. 4 Flow and shock geometry at Mach number lower than the design value, with MHD accelerator control.

An attractive scenario for MHD inlet control that has been analyzed by several groups[2,3,5–11] is to design the vehicle for a relatively low Mach number, for example, Mach 5 or 6, and, at high Mach numbers, move the shocks from inside the inlet back to the cowl lip by an MHD generator device placed at one of the compression ramps (Fig. 5). The advantages of this method are the following: 1) The vehicle size and weight can be reduced due to both absence of a mechanically variable inlet and the shortening of the compression

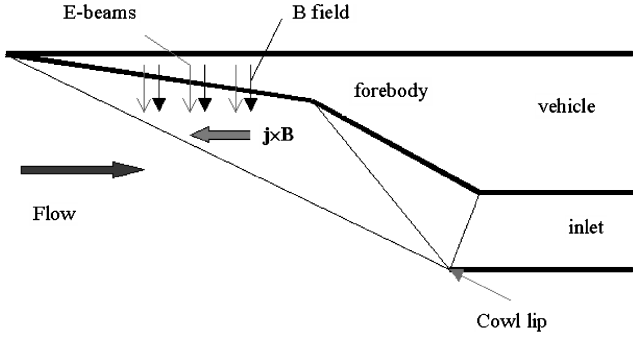

Fig. 5 Flow and shock geometry at Mach number higher than the design value, with MHD generator control.

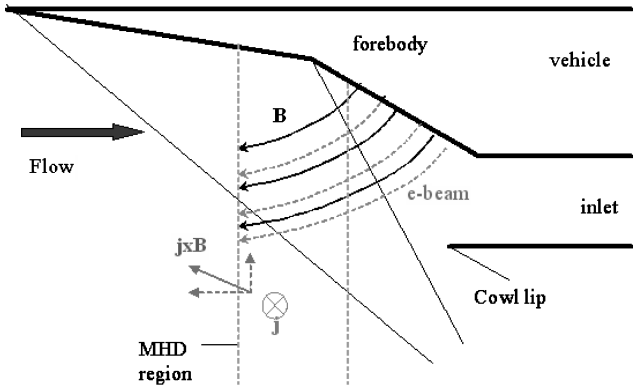

Fig. 6 Flow and shock geometry at Mach number lower than the design value, with MHD generator control.

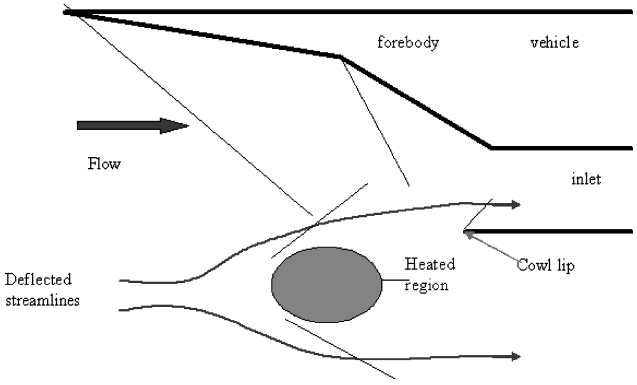

Fig. 7 Schematic diagram of the virtual cowl concept: off-body heat addition increases mass capture.

ramp. (The weight savings may offset the weight of the magnet and other MHD-related hardware.) 2) No net power is required to run the MHD device because the generator mode is used and the power requirements for air ionization can be minimized with electron beams as ionizers. 3) There is flexibility of flow control. An important disadvantage of this approach is that the inevitable joule heating and other dissipative processes result in substantial stagnation pressure losses and no gains in mass capture.

In this paper, we focus on the inlet control at Mach numbers higher than the design value by means of an on-ramp MHD generator. The analysis builds on our earlier work. The principal new element in this paper is an analysis of MHD regions that are very short compared with both length and width of the vehicle forebody. This approach, as demonstrated in the paper, has several advantages in comparison with long MHD interaction regions considered earlier.

An important factor in the analysis is that, in the flight regime of interest, static temperature is too low for thermal ionization of

air. Therefore, nonequilibrium ionization in MHD devices must be done.[10–17] The energy cost of ionization imposes very rigid constraints on the choice of ionization methods: Only the most energetically efficient ionization method can be used in these devices. Our earlier work showed that electron beams injected into the gas along magnetic field lines constitute the most efficient way of creating nonequilibrium ionization.[10–17] However, even with the most efficient ionizer, the very existence of ionization cost does not allow the ionization degree and the conductivity in hypersonic MHD devices to be very high.[10–17] This makes the task of using MHD for hypersonic flow control and power generation quite challenging.

II. Model

We consider hypersonic gas flow along a series of compression ramps upstream of the inlet with a forward-shifted cowl lip, as schematically shown in Figs. 1–7. The flow is two dimensional in the (x, z) plane, where x is the freestream flow direction and z is directed from the vehicle nose downward. Cases both without and with MHD influence on the flow are computed. In MHD cases, both magnetic field and ionizing electron beam are directed parallel to z axis. Because the entire flow region is hypersonic, a steady-state solution using x as a marching coordinate can be found.

The set of Euler equations in Cartesian coordinates, together with an ideal gas equation of state, a simple model of an ideal Faraday MHD generator, vibrational relaxation, and a plasma kinetic model are those of Refs. 10 and 11. In the present paper, we solve steady-state problems only, so that all time derivatives in the equations of Ref. 11 were equated to zero.

Power deposition and ionization by the electron beams have to be coupled with gasdynamic and plasma kinetic equations. In our earlier work,[13–17] we used the so-called forward–backward approximation[18] for electron beam propagation along magnetic field lines into gases and beam-generated ionization. This method is quite accurate, and it can be (and, in fact, was[13,14]) coupled with Navier–Stokes and MHD equations. However, computational demands of the full forward–back method, when coupled with gasdynamic and MHD equations, are prohibitive. Therefore, a simple but accurate way to predict ionization profiles was found.

Having analyzed the physics of ionization processes, we concluded that in a uniform gas the ionization rate profile has to be close to a truncated Gaussian. Indeed, ionization of molecules by electron impact is inefficient both at low and high (above 1 keV) electron energies.[19,20] The maximum of the ionization cross section corresponds to electron energy of several hundred electronvolts.[19,20] In this energy range, and even above it, the probability of backscattering is substantial, and there are both forward and backward electron fluxes exchanging electrons between them. The resulting motion is very much like diffusion. Thus, energy deposition Q_b and ionization profiles computed with both forward–back method and CYLTRAN Monte Carlo calculations[13,17] are very close to Gaussian profiles (Refs. 10 and 11):

$$Q_b(\xi) = a + (b/w)\exp\left[-2(\xi - z_m)^2 \big/ w^2\right] \tag{1}$$

where $\xi = z_b(x) - z$, $z_m \approx L_R/3.21$, $w \approx 1.64 z_m$, and $L_R(\varepsilon_b, N)$ is the beam relaxation length. There are two additional conditions for determining the constants a and b,

$$Q_b(L_R) = 0 \qquad \int_0^{L_R} Q_b(\xi)\,\mathrm{d}\xi = |j_b|\frac{\varepsilon_b}{e} \tag{2}$$

where ε_b and j_b are the beam electron energy and current density at the injection point.

The use of a loss function[10,11] or the direct solution of kinetic equation for electrons in the forward–back approximation give a relaxation length overestimated by a factor of 1.5–2. This is because lateral electron scattering and the loss of an additional energy equal to the energy of the secondary electron were neglected in those approximations. In the present paper, an empirical approximation formula for the electron beam relaxation length that effectively includes those two effects is used.

Assuming that the empirical approximation[21] for the beam relaxation length in a gas with uniform number density, $N = \text{const}$, is also valid for nonuniform neutral gas density, but with the average number density along the beam direction, $\bar{N}$, and that the relaxation length along magnetic field in dense gases is the same as without the magnetic field, we have for the relaxation length (in meters)

$$L_R = 1.1 \times 10^{21} \varepsilon_b^{1.7} \big/ \bar{N} \tag{3}$$

where ε_b is in kiloelectron volts, $\bar{N}$ is in 1/(cubic meter), and L_R is in meters. At each location along x, with the L_R in this location, we can find $\bar{N}(x)$ and $\varepsilon_b(x)$:

$$\bar{N}(x) = \frac{1}{L_R}\int_0^{L_R} N(\xi, x)\,\mathrm{d}\xi, \qquad \varepsilon_b(x) = \left(\frac{L_R \bar{N}}{1.1 \times 10^{21}}\right)^{1/1.7} \tag{4}$$

Equations (1–4) fully determine both beam-induced profiles: energy deposition Q_b and ionization rate,

$$q_i(x, \xi) \approx Q_b(x, \xi)/(eW_i) \tag{5}$$

where $W_i = 34$ eV is the energy cost of ionization by high-energy beam.

To facilitate the performance assessment of the propulsion system with and without MHD control, in addition to the total enthalpy flux $\dot{H}$ in watts per meter in the spanwise direction, the following dimensionless parameters were computed at the inlet throat (throat indicated by vertical arrows subsequently); mass capture ratio k_m; total pressure ratio k_{p_t}; total enthalpy ratio k_H; static pressure, density, and temperature ratios k_p, k_ρ, and k_T; adiabatic and cooled kinetic energy efficiencies $\eta_{\mathrm{KE,ad}}$ and $\eta_{\mathrm{KE,cool}}$; and the average Mach number M. (Note that the detailed assessment is outside the scope of the present work.) The coefficients k for mass flow rate and total and static pressures, temperatures, etc., are the ratios of the respective dimensional values at the throat to the freestream values. Note that mass capture k_m is calculated by referencing the actual mass flow rate at the throat to the mass flow rate through the inlet capture area at zero angle of attack. With this definition, k_m can exceed 1.

One problem in expressing the results in terms of the mentioned set of parameters is that in most cases the flow at the inlet throat is quite nonuniform. Therefore, a proper procedure of averaging flow parameters at the throat has to be employed. In this work, we use the so-called stream-thrust averaging commonly accepted in inlet design.[1] This procedure, described in Ref. 1, effectively takes into account losses of total pressure (entropy increase) that would occur in the isolator when the flow is allowed to settle and to become parallel to the walls.

III. MHD Control at $M > M_{\mathrm{design}}$: Methodology of Computations

The two-dimensional, four-ramp inlet geometry, designed for Mach 5 flight at 2-deg angle of attack, is shown in Fig. 8. The ramp angles are 2.5, 8.5, 11, and 13 deg. The location of the cowl lip was chosen so that the first three oblique shocks would together reach the point slightly upstream of the lip (barely missing the lip); the fourth shock was allowed to hit the cowl. The freestream conditions at all Mach numbers studied correspond to the flight dynamic pressure of 2000 psf (95,760.5 Pa, or about 1 atm). Table 1 lists freestream

Table 1 Freestream parameters[a] in computed cases

Mach number	h, km	p_0, Pa	T_0, K
5	20.066	5472	216.65
6	22.47	3800	218.98
7	24.407	2791.84	220.96
8	26.155	2137.5	222.70
10	29.108	1368	225.63

[a]Freestream dynamic pressure is $q = 2000$ psf.

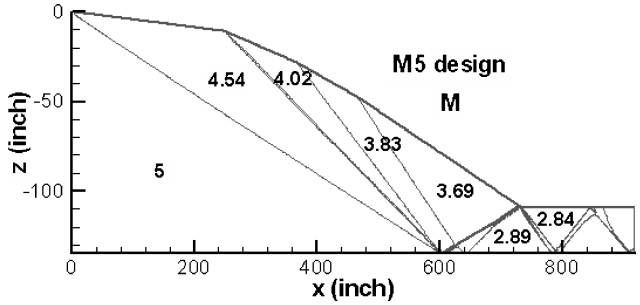

a)

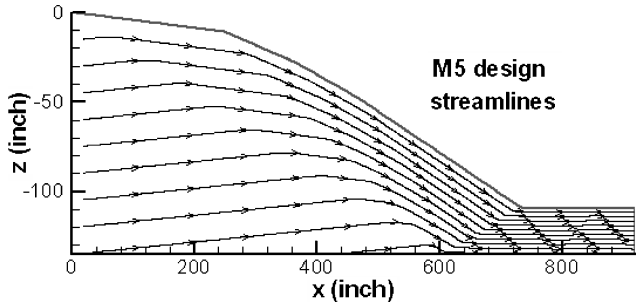

b)

Fig. 8 Mach 5 design case: a) Mach number contours and b) streamlines.

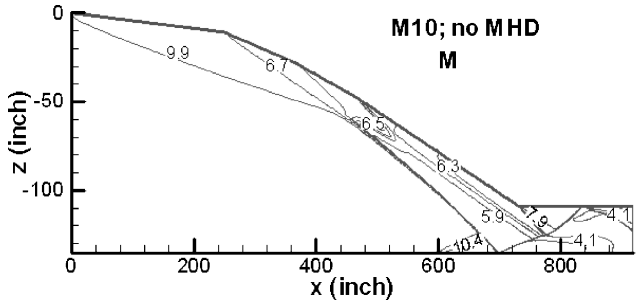

a)

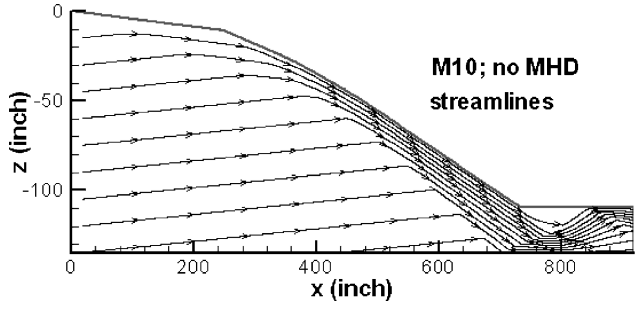

b)

Fig. 9 Mach 10 case without MHD control where geometry is that of Fig. 8: a) Mach number contours and b) streamlines.

conditions, altitude h, and static pressure and temperature, p_0 and T_0, in all computed cases.

At Mach numbers greater than 5, the shocks would make contact with the cowl, reducing total pressure at the inlet, and potentially causing very high heat transfer rates at the shock incidence point, and possibly flow separation and engine unstart. The shock pattern and flow streamlines at off-design Mach 10 are shown in Fig. 9. As seen in Fig. 9b, the flow in the inlet is not parallel to the walls.

To maximize performance in MHD control cases, the magnetic field should be as strong as possible and it should protrude from the ramp into the flow as far as possible. The field was assumed to be generated by a set of large-diameter superconducting coils placed inside the forebody and projecting magnetic field downward. The maximum field strength at the end plane of the coil was assumed to be 3.7 T, so that the field at the ramp surface is 3.5 T. The field outside the coil is a function of the ratio of the distance from the coil end plane and the coil radius, as shown in Fig. 10 (courtesy of G. Naumovich of Everson Magnetics). Thus, the protrusion of the B field into the gas increases with the coil diameter. The latter is obviously limited by the span (width) of the forebody. In the present work, the coil diameter was assumed to be 5 m. This, together with the maximum field at the ramp, determined the centerline magnetic field as a function of vertical coordinate z, in accordance with Fig. 10.

Off the centerline, the B field is not only reduced in magnitude, but it also diverges. Therefore, to maximize the Lorentz forces pushing the flow and shocks upstream, the MHD interaction region should be concentrated near the centerline of the coil.

The ionization of air in the MHD region is created by electron beams injected from the ramp along magnetic field lines. Concentrating electron beam current in a short region near the magnet centerline would avoid the need to have a large area of the vehicle surface covered by fragile windows or differentially pumped ports, which would have been required in cases of long, distributed MHD interaction regions. As the MHD interaction length L becomes short, the electrical conductivity σ has to be increased to keep the interaction parameter (Stuart number) $S = \sigma B^2 L/\rho u$ (where ρ and u are the flow density and velocity), at the same level as that for long, distributed MHD region. Because the ionization fraction and the conductivity are proportional to the square root of electron beam current density, shortening the MHD region from 2–3 m down to 10–20 cm requires increasing the beam current density by two orders of magnitude, to 50–100 mA/cm^2. Aerodynamic windows or differentially pumped plasma portholes may be good candidates for electron beam transmission. Such windows or ports can presumably handle very high electron beam currents, even much higher than 100 mA/cm^2, in contrast to conventional thin foils. Although, in practice, there may have to be multiple beam transmission slots in 10–20 cm long MHD region, in this work we assume for simplicity that the electron beam current density is uniform along the MHD region.

For the best performance, the MHD interaction region should be placed as far upstream as possible. Indeed, the required linear shift of the shock incidence point at the cowl level is caused by a smaller change in shock angle and, therefore, by a lower MHD interaction parameter, when the MHD region is moved upstream. Additionally, creating the necessary level of ionization at lower gas density (closer to freestream conditions) requires lower current density and power of the ionizing electron beams. The two requirements for the placement of the MHD interaction region (that the interaction region should be as far upstream as possible and that it should be close to the magnetic coil centerline) define the minimum distance of about one-half forebody span (in our cases, about 2.5 m) of the beginning of the MHD interaction region from the nose. To allow some room for the magnet inside the forebody, this distance was increased to 3.5 m.

In the considered geometry, the Faraday-induced electric current flows in the spanwise direction. One way of collecting that current is to extend sidewalls up to the MHD region and to have electrodes imbedded in the sidewalls. In the present paper, we leave the design and mechanical and thermal management issues associated with sidewalls aside. We also assume the MHD region to be an ideal Faraday generator. The latter assumption is nontrivial. The Hall parameters in the computed cases can reach as high as 10. In conventional Faraday channels with continuous electrodes, MHD effects are sharply reduced due to the Hall effect, whereas in Faraday channels with segmented electrodes there is a danger of arcing between the electrode segments at high Hall parameters. However, the MHD devices analyzed in this work are very different from conventional devices. Not only is the conductivity nonthermal and generated and controlled by externally injected electron beams, but also the length of the channel (15–30 cm) is much shorter than its width (5 m). Considering short MHD channel as a slice of a long

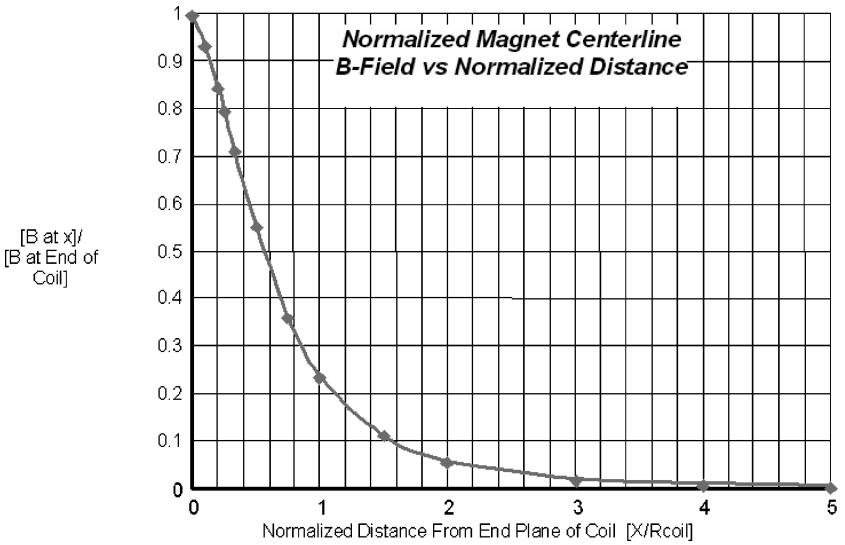

Fig. 10 Normalized magnetic field along coil centerline vs normalized distance from end plane of coil (courtesy of G. Naumovich, Everson Magnetics).

channel, with only one electrode segment, one might argue that the performance of such a short channel should be close to that of an ideal Faraday device, even at high Hall parameters. This argument requires an investigation and validation, which is outside the scope of this paper.

In all computed cases, an ideal Faraday generator was assumed. In most cases, the load factor was set at $k = 0.5$, and variation of the computed parameters with varying k was studied for Mach 10 case (shown subsequently).

The task of an on-ramp MHD device is to push at least the nose shock just outside the cowl lip. With the location of the beginning of MHD region and the B field profile determined by the analysis in the preceding paragraphs, and at a fixed load factor k, an additional constraint was imposed by setting the electron beam current density at $j_b = 100$ mA/cm^2 for Mach 7–10 and $j_b = 25$ mA/cm^2 for Mach 6. Because the beam power required to sustain a certain conductivity scales as the square of the conductivity, whereas the power extracted by MHD is proportional to the conductivity, these beam current densities are close to the maximum values for self-powered MHD device, that is, where the power spent on ionization does not exceed the MHD-extracted power.

The beam energy as a function of distance along the flow was selected to maintain a constant extrapolated beam relaxation length L_R [Eq. (3)]. From preliminary calculations, the extrapolated relaxation length $L_R = 2.22$ m was chosen as close to the optimum value. At relaxation lengths shorter than the chosen value, the interaction region is too close to the ramp, and a substantial portion of the flow experiences little MHD effect. On the other hand, at $L_R > 2.22$ m, electron beams penetrate into the gas too far and generate a plasma in the region where the magnetic field is too weak for substantial MHD effects. Note that the specific numerical value of L_R would be different with a different vehicle geometry.

With this selection of parameters, the length of the MHD region is the only variable. This length was determined in the calculations as the minimum MHD interaction length that pushes at least the first (nose) shock, and perhaps the second shock, back just outside the cowl lip.

IV. Results and Discussion

Figure 11 shows the variation of electron beam energy ε_b with distance along the flow, x, and also shows the length of the MHD region. The interaction length varies from 15 cm at Mach 7–30 cm at Mach 10, and the beam energy range is about 60–110 keV.

Figures 12–19 show contour lines of flow and plasma parameters in the Mach 10 case with MHD interaction. (At other Mach numbers, the pattern is qualitatively similar.) Note that, although the

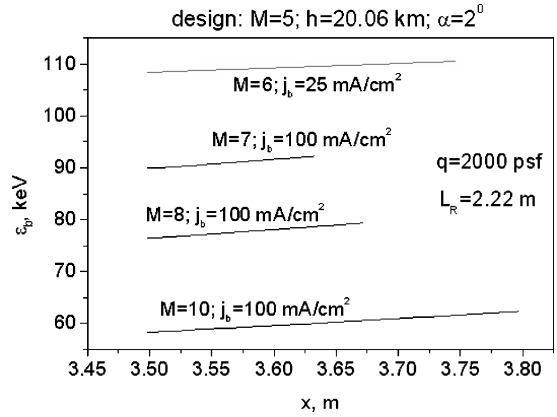

Fig. 11 Electron beam energy vs distance from nose of vehicle.

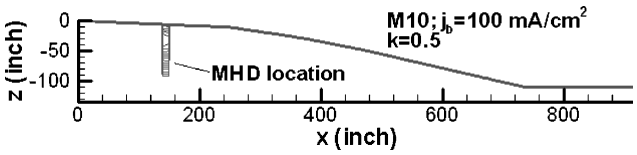

Fig. 12 Location of MHD interaction region for Mach 10 case with MHD control where geometry is that of Fig. 8.

MHD interaction region may look like a discontinuity in Figs. 14 and 15, this impression is due to the scale used because the interaction region has a macroscopic thickness of 30 cm (Figs. 16–19). However, because the thickness is much smaller than other length scales of the problem, it might be possible, in principle, to substitute the MHD interaction region by a discontinuity and to derive the appropriate jump conditions that would, of course, be quite different from Rankine–Hugoniot conditions and that would depend on parameters of electron beams, magnetic field, and load factor.

Table 2 lists the computed inlet parameters in MHD and non-MHD cases. Table 3 contains the principal MHD parameters: the load factor k, the rate of work by $\boldsymbol{j} \times \boldsymbol{B}$ forces, $P_{j \times B}$; the extracted power P_{MHD}; the gas heating rate P_J; the power deposition into vibrational mode of molecules, P_V; the power of ionizing electron beams, P_b; the MHD interaction parameter S; the enthalpy extraction ratio η; the total Faraday current I_y; and the maximum longitudinal (Hall) electric field $E_{x,\max}$. Note that due to two dimensionality of the problem, all power quantities P are expressed per unit length (1 m) in the spanwise direction.

Table 2 Computed inlet parameters[a] with and without MHD control for Mach 5 design

Freestream Mach no. and MHD conditions	k_m	k_{p_t}	k_H	k_p	k_ρ	k_T	M	$\eta_{\mathrm{KE,ad}}$	$\eta_{\mathrm{KE,cool}}$	$\dot{H}$, MW/m
$M = 5$, design, no MHD	1.13	0.855	1	16.01	6.932	2.31	2.825	0.990	0.991	661.3
$M = 6$ no MHD	1.13	0.635	1	17.36	6.74	2.57	3.3	0.980	0.980	758.4
MHD,[b] $k = 0.5$	1.116	0.531	0.998	18.53	6.72	2.75	3.14	0.972	0.971	742.4
$M = 7$ no MHD	1.13	0.448	1	19.47	6.63	2.94	3.65	0.973	0.973	856.1
MHD,[c] $k = 0.5$	1.13	0.344	0.997	22.20	6.77	3.27	3.379	0.964	0.961	852.0
$M = 8$ no MHD	1.13	0.316	1	22.01	6.54	3.36	3.94	0.969	0.969	957.2
MHD,[c] $k = 0.5$	1.13	0.226	0.986	25.97	6.79	3.82	3.57	0.960	0.945	952.1
$M = 10$ no MHD	1.12	0.161	1	28.1	6.43	4.37	4.36	0.966	0.966	1163
MHD,[c] $k = 0.5$	1.115	0.107	0.933	32.35	6.785	4.77	3.94	0.961	0.891	1103
$k = 0.25$	1.11	0.106	0.933	32.37	6.76	4.78	3.93	0.961	0.891	1099
$k = 0.75$	1.11	0.104	0.939	32.73	6.74	4.85	3.91	0.960	0.896	1103
$k = 0.5$ downstream	1.05	0.04	0.928	49.83	7.0	7.1	2.95	0.933	0.858	1037

[a]Angle of attack is 2 deg, and flight dynamic pressure is $q = 2000$ psf. [b]Current density $j_b = 25$ mA/cm^2. [c]Current density $j_b = 100$ mA/cm^2.

Table 3 Computed MHD parameters

Freestream Mach no.	k	$P_{j\times B}$ MW/m	P_{MHD}, MW/m	P_J, MW/m	P_V, MW/m	P_b, MW/m	S	η	I_y, kA	$E_{x,\max}$, kV/m
6	0.5	15.3	7.6	7.7	$\ll 1$	6.817	0.038	0.01	3.858	8.78
7	0.5	26.63	13.31	12.73	0.58	12.35	0.056	0.015	5.698	13.15
8	0.5	43.57	21.78	18.69	3.095	15.47	0.084	0.022	8.379	19.05
10	0.5	105.8	52.89	32.28	20.6	18.01	0.173	0.044	16.76	36.76
10	0.25	105.6	26.39	37.22	41.96	13.53	0.115	0.022	16.73	55.14
10	0.75	100.9	75.72	22.28	2.961	28.59	0.328	0.063	15.97	18.38
10	0.5 downstream	131.3	65.63	44.9	20.74	28.84	0.212	0.055	21.99	32.24

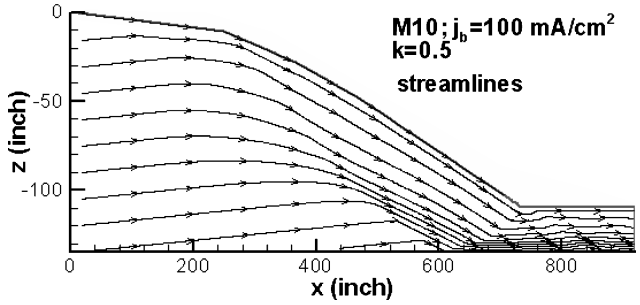

Fig. 13 Flow streamlines for Mach 10 case with MHD control, where geometry is that of Fig. 8.

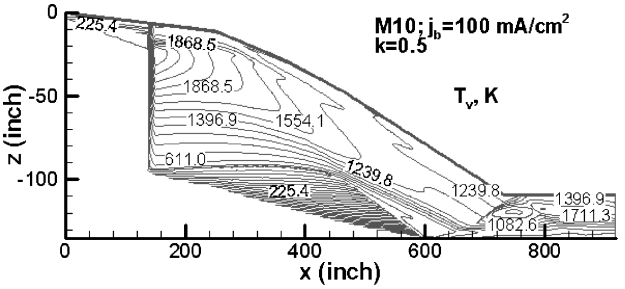

Fig. 15 Contour lines of vibrational temperature for Fig. 12 case.

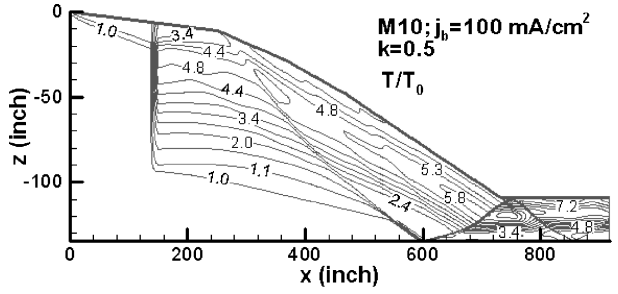

Fig. 14 Contour lines of static temperature nondimensionalized by freestream static temperature for Fig. 12 case.

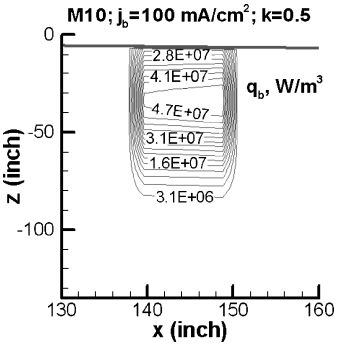

Fig. 16 Contour lines of electron beam power deposition for Fig. 12 case.

Tables 2 and 3 list, among other quantities, the computed parameters in Mach 10 MHD cases with three different load factors, and Fig. 20 shows the beam energy as a function of distance from the nose and the lengths of the MHD region in the three cases. As seen in Tables 2 and 3, with proper optimization, inlet parameters are quite close in all three cases. However, the power spent on ionization by electron beams, P_b, and the extracted power P_{MHD} are different in the three cases. At low value of load factor, $k = 0.25$, P_b becomes a larger fraction of P_{MHD} than at $k = 0.75$ and $k = 0.5$. Thus, the optimum load factor should not be too low. In fact, the highest of the three values of k, that is, $k = 0.75$, appears to yield the best performance: the largest net extracted power $P_{\mathrm{MHD}} - P_b$ and the weakest Hall electric field. This trend of better performance at higher load factors should be explored, and the optimum k determined, in future work. Note, however, that increasing k requires lengthening of the MHD region (Fig. 20); thus, attempts to improve performance

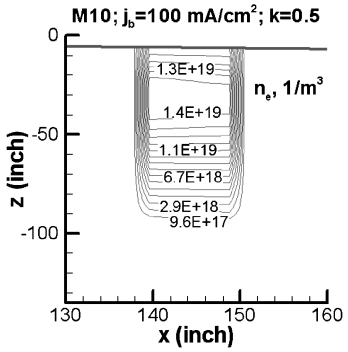

Fig. 17 Contour lines of electron number density for Fig. 12 case.

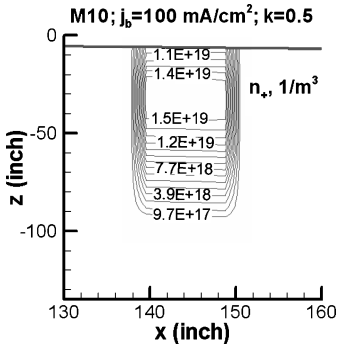

Fig. 18 Contour lines of positive ion number density for Fig. 12 case.

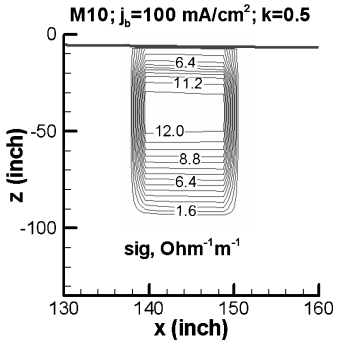

Fig. 19 Contour lines of electrical conductivity for Fig. 12 case.

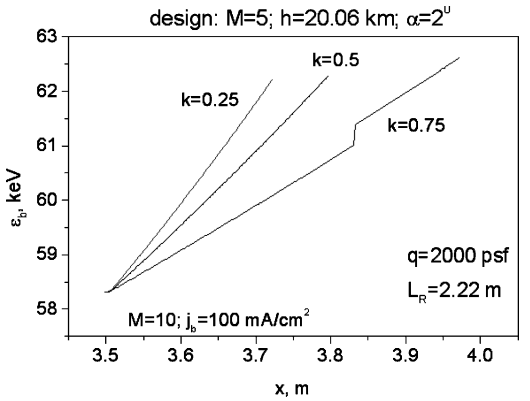

Fig. 20 Electron beam energy vs distance from the nose of the vehicle at different load factors in Mach 10 case with MHD control, where geometry and MHD location are those of Fig. 12.

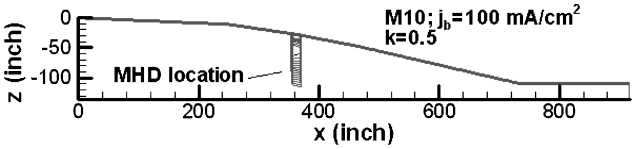

Fig. 21 Downstream location of MHD region in Mach 10 case with MHD control, where geometry is that of Figs. 8 and 12.

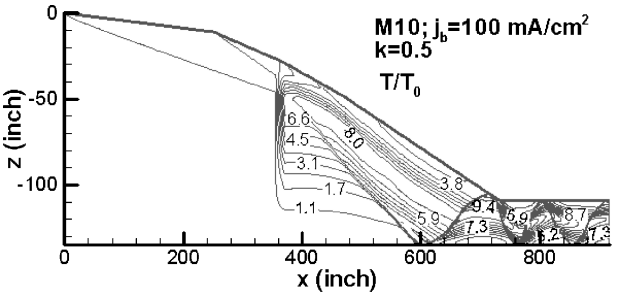

Fig. 22 Contour lines of static temperature nondimensionalized by freestream static temperature in Fig. 21 case.

by increasing the load factor can be limited by a weakening and diverging magnetic field off the coil centerline.

To check the variation of performance with position of the MHD interaction region, calculations were also performed at Mach 10, $k = 0.5$, for MHD region beginning farther downstream from the nose (Figs. 21 and 22). Table 2, where the results of this calculation are compared with those for the upstream location of the MHD region, demonstrates that the upstream location is indeed preferred because it gives better results in terms of mass capture, total pressure, and kinetic energy efficiency.

As seen in Tables 1–5, MHD inlet control is inevitably accompanied by losses of total pressure and kinetic energy efficiency. These losses are due to entropy generation by dissipative joule heating and to extraction of flow energy in the form of work (electric power). Although the dissipative processes are certainly irreversible, the extracted work (minus the cost of ionizing electron beams and various losses) can, in principle, be used to augment the thrust of the propulsion system, thus, partially compensating for the losses of total pressure in the on-ramp MHD generator. Specifically, the total rate of work by $\boldsymbol{j} \times \boldsymbol{B}$ forces, $P_{j \times B}$, is spent on 1) irreversible joule heating that consists of gas heating in the narrow sense, P_J, and the power deposition into vibrational mode of molecules, P_V, and 2) the generated electric power P_{MHD} : $P_{j \times B} = P_{\mathrm{MHD}} + (P_J + P_V)$. The ratio between the extracted power and the rate of dissipation is determined by the load factor. At $k = 0.5$, $P_{\mathrm{MHD}} = P_J + P_V = 0.5 P_{j \times B}$. A part of the extracted power must be spent on electron beams, so that the available power is $(P_{\mathrm{MHD}} - P_b)$; in practice, there will be some losses in both beam generation and power conditioning and transfer. The remaining net power can be spent, in part, to power various onboard devices and, in part, to augment the propulsion by either energy addition in the combustor or by operating an MHD accelerator downstream of the combustor. The latter option can be viewed as a modified version of MHD bypass concept. In this version, energy bypass ratio is quite low, a few percent, and the primary purpose of MHD generator is to control and optimize the inlet; because in the process of inlet control net power can be generated, that power can be in principle used in a downstream MHD accelerator to compensate partially for the loss of stagnation pressure in the MHD generator. Although stagnation pressure is still decreased by irreversible processes, the benefits of such an approach may come from effective inlet management and potential weight savings due to the absence of hydraulic cowl control and the shortened forebody (provided that a lightweight magnet technology can be developed).

All computations in this work were performed with $12{,}500 \times 120$ rectangular grid. To check how sensitive the results are to the grid size, selected cases were computed with a coarser grid. The variation of the results with grid size, listed in Tables 4 and 5, was quite small.

Table 4 Variation of computed inlet performance parameters at Mach 10, 2000 psf, with grid size[a]

Case	k_m	k_{p_t}	k_p	k_ρ	k_T	M	$\eta_{\mathrm{KE,ad}}$	η_{KE}	$\dot{H}$, MW/m
No MHD	1.12	0.1614	28.1	6.43	4.37	4.36	0.9658	0.9659	1163
	(1.1)[a]	(0.1611)	(27.68)	(6.36)	(4.35)	(4.37)	(0.9657)	(0.9663)	(1150)
MHD, $k = 0.5$	1.115	0.107	32.35	6.785	4.768	3.94	0.9617	0.8912	1103
	(1.114)	(0.109)	(32.03)	(6.771)	(4.729)	(3.96)	(0.9621)	(0.8916)	(1102)

[a]Coarser grid, 7500×90.

Table 5 Variation of computed MHD parameters with grid size[a]

Grid	$P_{j\times B}$, MW/m	P_{MHD}, MW/m	P_J, MW/m	P_V, MW/m	P_B, MW/m	S	η	I_y, kA	$E_{x,\max}$, kV/m
$12{,}500 \times 120$	105.78	52.89	32.28	20.6	18.01	0.173	0.044	16.762	36.757
$7{,}500 \times 90$	105.16	52.58	32.01	20.57	17.92	0.1742	0.0438	16.665	36.521

[a]Mach 10, 2000 psf, load factor $k = 0.5$, and electron beam current density of 100 mA/cm^2.

V. Conclusions

Among various scenarios of scramjet inlet control, this paper focused on the on-ramp MHD generator that would bring the shocks back on lip at Mach numbers greater than the design value. Compared with the earlier work, here we emphasized and used advantages of a very short (15–30-cm) MHD interaction region. The performance of the short MHD region is enhanced by operating upstream, at the first compression ramp, and by using the strongest magnetic field near the coil centerline. Additionally, having differentially pumped aerodynamic windows for electron beam transmission in only a small portion of the ramp surface alleviates structural problems, while allowing transmission of high beam current densities. We also argued that the performance of an MHD channel whose length is short compared with its width should approach that of an ideal Faraday device. This latter idea needs further investigation and validation.

The MHD inlet control device is self-powered, with ionization cost substantially lower than the generated power. Among its problems are the weight and bulk of magnets and power systems and losses of stagnation pressure due to joule heating and power extraction. Note that the stagnation pressure losses can, in principle, be partially compensated with energy bypass: The generated electricity can be used for MHD acceleration of the flow in the combustor or downstream of it. If a lightweight magnet technology can be developed, overall weight savings may result from avoiding a mechanical system of variable geometry inlet and from a shorter forebody designed for lower Mach numbers. Thus, the viability of MHD inlet control can only be determined in detailed system studies.

Acknowledgments

This work was supported by Boeing Phantom Works, by the Johns Hopkins University, Applied Physics Laboratory, and by the Air Force Office of Scientific Research. The authors express their gratitude to Joseph Silkey and Philip Smereczniak of Boeing Phantom Works, to David Van Wie of the Johns Hopkins University, Applied Physics Laboratory, to Ramon Chase of ANSER, and to Daniel Swallom of Textron, Inc., for guidance, valuable discussions, and advice.

References

[1]Van Wie, D. M., "Scramjet Inlets," *Scramjet Propulsion*, edited by E. T. Curran and S. N. B. Murthy, Vol. 189, Progress in Astronautics and Aeronautics, AIAA, Reston, VA, 2000, Chap. 7, pp. 447–511.

[2]Shneider, M. N., Macheret, S. O., and Miles, R. B., "Nonequilibrium Magnetohydrodynamic Control of Scramjet Inlets," AIAA Paper 2002-2251, May 2002.

[3]Kuranov, A. L., and Sheikin, E. G., "MHD Control on Hypersonic Aircraft under AJAX Concept: Possibilities of MHD Generator," AIAA Paper 2002-0490, Jan. 2002.

[4]Macheret, S. O., Shneider, M. N., and Miles, R. B., "Scramjet Inlet Control by Off-Body Energy Addition: a Virtual Cowl," AIAA Paper 2003-0032, Jan. 2003.

[5]Vatazhin, A., Kopchenov, V., and Gouskov, O., "Some Estimations of Possibility to Use the MHD Control for Hypersonic Flow Deceleration," AIAA Paper 99-4972, June 1999.

[6]Kopchenov, V., Vatazhin, A., and Gouskov, O., "Estimation of Possibility of Use of MHD Control in Scramjet," AIAA Paper 99-4971, June 1999.

[7]Vatazhin, A., Kopchenov, V., and Gouskov, O., "Numerical Investigation of Hypersonic Inlets Control by Magnetic Field," *The 2nd Workshop on Magneto- and Plasma Aerodynamics in Aerospace Applications*, Inst. of High Temperatures, Russian Academy of Sciences, Moscow, 2000, pp. 56–63.

[8]Brichkin, D. I., Kuranov, A. L., and Sheikin, E. G., "The Potentialities of MHD Control for Improving Scramjet Performance," AIAA Paper 99-4969, June 1999.

[9]Bityurin, V. A., Klimov, A. I., Leonov, S. B., Bocharov, A. N., and Lineberry, J. T., "Assessment of a Concept of Advanced Flow/Flight Control for Hypersonic Flights in Atmosphere," AIAA Paper 99-4820, Nov. 1999.

[10]Macheret, S. O., Shneider, M. N., and Miles, R. B., "External Supersonic Flow and Scramjet Inlet Control by MHD with Electron Beam Ionization," AIAA Paper 2001-0492, Jan. 2001.

[11]Macheret, S. O., Shneider, M. N., and Miles, R. B., "Magnetohydrodynamic Control of Hypersonic Flow and Scramjet Inlets Using Electron Beam Ionization," *AIAA Journal*, Vol. 40, No. 1, 2002, pp. 74–81.

[12]Macheret, S. O., Shneider, M. N., and Miles, R. B., "Magnetohydrodynamic and Electrohydrodynamic Control of Hypersonic Flows of Weakly Ionized Plasmas," *AIAA Journal*, Vol. 42, No. 7, 2004, pp. 1378–1387.

[13]Macheret, S. O., Shneider, M. N., Miles, R. B., Lipinski, R. J., and Nelson, G. L., "MHD Acceleration of Supersonic Air Flows Using Electron Beam-Enhanced Conductivity," AIAA Paper 98-2922, June 1998.

[14]Macheret, S. O., Shneider, M. N., and Miles, R. B., "Electron Beam Generated Plasmas in Hypersonic MHD Channels," AIAA Paper 99-3635, June 1999.

[15]Macheret, S. O., Shneider, M. N., and Miles, R. B., "MHD Power Extraction from Cold Hypersonic Air Flow with External Ionizers," AIAA Paper 99-4800, Nov. 1999.

[16]Macheret, S. O., Shneider, M. N., and Miles, R. B., "MHD Power Extraction from Cold Hypersonic Air Flow with External Ionizers," *Journal of Propulsion and Power*, Vol. 18, No. 2, 2002, pp. 424–431.

[17]Macheret, S. O., Shneider, M. N., Miles, R. B., and Lipinski, R. J., "Electron Beam Generated Plasmas in Hypersonic Magnetohydrodynamic Channels," *AIAA Journal*, 2001, Vol. 39, No. 6, pp. 1127–1136.

[18]Raizer, Y. P., and Shneider, M. N., "Simplified Kinetic Equation for Electrons in Nonuniform Fields of Arbitrary Strength in Connection with the Cathode Sheath of a Glow Discharge," *Soviet Journal of Plasma Physics*, Vol. 15, No. 3, 1989, pp. 184–189.

[19]Berger, M. J., and Seltzer, S. M., "Tables of Energy Losses and Ranges of Electrons and Positrons," NASA SP-3012, 1964.

[20]Bychkov, Y. I., Korolev, Y. D., and Mesyats, G. A., *Injection Gaseous Electronics (Inzhektsionnaia Gazovaia Elektronika)*, Nauka, Moscow, 1982, Chap. 2 (in Russian).

[21]Bychkov, V. L., Vasilev, M. N., and Zuev, A. P., "An Experimental and Theoretical Investigation of the Properties of Surface Electron-Beam Nitrogen Plasma," *High Temperature*, Vol. 32, No. 3, 1994, pp. 303–312.

G. Candler
Associate Editor